Original Article

Impact Assessment of Systemic Geometric Distortion in 1.5T Magnetic Resonance Imaging Simulation through Three-dimensional Geometric Distortion Phantom on Dosimetric Accuracy for Magnetic Resonance Imaging-only Prostate Treatment Planning

Korawig Chaknam[1], Ladawan Worapruekjaru[2], Sithiphong Suphaphong[2], Nualjun Stansook[2], Prapa Sodkokkruad[1], Sawwanee Asavaphatiboon[1]

[1]Division of Diagnostic Radiology, Department of Diagnostic and Therapeutic Radiology, [2]Division of Radiation Oncology, Department of Diagnostic and Therapeutic Radiology, Faculty of Medicine Ramathibodi Hospital, Mahidol University, Bangkok, Thailand

Abstract

Aims: Magnetic resonance imaging (MRI)-only radiotherapy has emerged as a solution to address registration errors that can lead to missed dose delivery. However, the presence of systemic geometric distortion (SGD) stemming from gradient nonlinearity (GNL) and inhomogeneity of the main magnetic field (B_0) necessitates consideration. This study aimed to quantitatively assess residual SGD in 1.5T MRI simulation using a three-dimensional (3D) geometric distortion phantom and evaluate its impact on dosimetric accuracy for retrospective prostate cancer patients. **Materials and Methods:** Ten retrospective cases of prostate cancer patients treated with volumetric modulated arc radiotherapy (VMAT) were randomly selected. A geometric distortion phantom was scanned on a 1.5T MRI simulation using a 3D T1 volumetric interpolated breath-hold examination sequence, varying bandwidth (BW), and two-phase-encoding directions. Distortion maps were generated and applied to the original computed tomography (oriCT) plan to create a distorted computed tomography plan (dCT), and a dice similarity coefficient (DSC) was observed. Dosimetric accuracy was evaluated by recalculating radiation dose for dCT plans using identical beam parameters as oriCT. **Results:** The SGD increased with distance from the isocenter in all series. DSC exceeded 0.95 for all plans except the rectum. Regarding GNL's impact on dosimetric accuracy, most mean percentage errors for clinical target volume, planning target volume, and both femurs were under 2% in all plans, except for the bladder and rectum. **Conclusion:** SGD pre-evaluation is crucial and should be incorporated into a quality assurance program to ensure effective MRI-simulation performance before MRI-only treatment planning for prostate cancer.

Keywords: Dosimetric accuracy, magnetic resonance imaging-only treatment planning, magnetic resonance imaging-simulation, systemic geometric distortion

Received on: 21-03-2024 **Review completed on:** 09-04-2024 **Accepted on:** 24-04-2024 **Published on:** 21-09-2024

Introduction

Magnetic resonance imaging (MRI) is increasingly integrated into radiotherapy workflows due to its high spatial soft-tissue contrast that improves the delineation of targets and organs at risk (OARs), especially in homogeneous tissue areas such as the head–neck and pelvic area.[1,2] However, image registration has the potential for systemic error stemming from misalignments between two image datasets. Consequently, MRI-only radiotherapy workflows have been developed to address this concern.[2-7] Nonetheless, MRI images are susceptible to geometric distortion. This phenomenon results

Access this article online

Quick Response Code:

Website: www.jmp.org.in

DOI: 10.4103/jmp.jmp_62_24

Address for correspondence: Asst. Prof. Sawwanee Asavaphatiboon, Department of Diagnostic and Therapeutic Radiology, Division of Diagnostic Radiology, Faculty of Medicine Ramathibodi Hospital, Mahidol University, 270 Rama Vi Road, Ratchathewi, Bangkok 10400, Thailand.
E-mail: sawwanee.medphy@gmail.com

How to cite this article: Chaknam K, Worapruekjaru L, Suphaphong S, Stansook N, Sodkokkruad P, Asavaphatiboon S. Impact assessment of systemic geometric distortion in 1.5T magnetic resonance imaging simulation through three-dimensional geometric distortion phantom on dosimetric accuracy for magnetic resonance imaging-only prostate treatment planning. J Med Phys 2024;49:356-62.

in structure distortion and affects the accuracy of radiation dose delivery.[1,4,8,9] This distortion becomes particularly critical in the context of a small target for stereotactic radiosurgery, as it may result in underdosage by as much as 30%.[10]

Geometric distortion mainly contributes to systemic geometric distortion (SGD) and objected-induced distortion (OID). SGD originates within the system itself and comprises gradient nonlinearity (GNL) and inhomogeneity of the main magnetic field (B_0). GNL increases in magnitude with increasing distance away from the magnet bore isocenter. On the other hand, the OID is associated with materials or tissues under the magnetic field, each possessing distinct magnetic susceptibility characteristics. The magnitude of OID depends on increasing magnetic field strength and is specific to an individual patient. The field of view (FOV) influences the degree of geometric distortion arising from the GNL, which is the principal source of SGD, surpassing OID. Correspondingly, GNL is the primary source of geometric distortion.[3,4,11-15] In particular, vendors offer distortion correction software to address SGD, albeit only partially. Hence, residual SGD necessitates consideration when evaluating the machine's performance. Therefore, this study aims to characterize the effect of different bandwidths (BWs) on the geometric distortion and assess the dosimetric accuracy from the impact of residual distortion of 1.5T MRI simulation by creating a distorted computed tomography (dCT) to compare against the original computed tomography (oriCT) plan for MRI-only prostate treatment planning.

Materials and Methods

Geometric distortion acquisition

An MRID^{3D} geometric distortion phantom (QUASAR™, Modus Medical, Canada) underwent scanning using a three-dimensional (3D) T1 volumetric interpolated breath-hold examination pulse sequence (410 mm × 420 mm FOV, 1.2 mm^3 isotropic voxel, single excitation, and enabled vendor's 3D geometric distortion correction) on 1.5T MRI simulation (MAGNETOM Aera, Siemens Healthcare, Erlangen, Germany). The scan covered the phantom's full dimensions (370 mm in diameter and 320 mm in length). The pulse sequence was designed to represent the worst-case scenario of residual distortion. The inverse gradient method facilitated the separation of GNL and B_0 inhomogeneity.[11,16] To investigate the effect of different BWs on geometric distortion, five BWs were tested at 130, 200, 380, 680, and 840 Hz/pixel. Subsequently, the acquired phantom images were imported into the MRID^{3D} geometric distortion software analysis system, where the 3D distortion vector field was calculated by the software algorithm. Images with opposite gradient polarity (e.g., anteroposterior (AP) and posteroanterior, right–left (RL), and left–right) were selected to separate the distortion source into GNL and B_0 inhomogeneity. The software provided statistical measures of absolute radial distortion from the magnet isocenter (mean, standard deviation, and maximum distortion). Then, distortion induced from GNL was used to generate distortion maps for each BW and phase-encoding direction.

Distorted computed tomography plan generation

The workflow demonstrated the generation of the dCT plan to compare with the original plan for dosimetric evaluation, as shown in Figure 1.

Ten retrospective prostate cancer patient treatment plans using volumetric modulated arc radiotherapy (VMAT) were randomly selected from the hospital's records spanning from 2020 to September 2022. To simulate SGD effects on the patient plan, distortion maps with varying BWs and phase-encoding directions were applied to the oriCT images of each patient using the MICE Toolkit (NONPI Medical AB, Umeå, Sweden). Furthermore, the distortion map's central coordinates were translated back to their oriCT location to maintain spatial consistency.

The original Radiotherapy (RT) structure was then deformed onto the dCT images for each patient using deformable image registration (DIR) within the treatment planning system (TPS: Eclipse, Varian Medical Systems, Palo Alto, CA). The radiation plan parameters were identically used as the oriCT plan. Subsequently, the radiation dose was recalculated without re-optimization for the dCT plan while keeping the monitor unit fixed. Evaluation of contour overlap between the dCT and oriCT plans was conducted using the dice similarity coefficient (DSC), where a DSC of 0 indicates no overlap, and 1 indicates a perfect overlap. Moreover, a radiation oncologist did not review the contour after DIR. According to the AAPM-TG132 recommendations, a DSC value >0.8–0.9 is acceptable.[17] Therefore, a cutoff criterion was established, with the DSC value below 0.9 for all structures to indicate inadequate performance. After applying the cutoff criterion, the average of the absolute percentage dose error (%Dose error) and DSC were calculated across the remaining structure.

Dosimetric accuracy evaluation

The assessment of dosimetric accuracy involved the calculation of the %Dose error between the dose of the dCT (D_{dCT}) and the dose of the oriCT (D_{oriCT}) according to the dose volume histogram (DVH). The %Dose error was determined using the following equation:

$$\%Dose\ error = \left| \frac{D_{oriCT} - D_{dCT}}{D_{oriCT}} \right| \times 100 \quad (1)$$

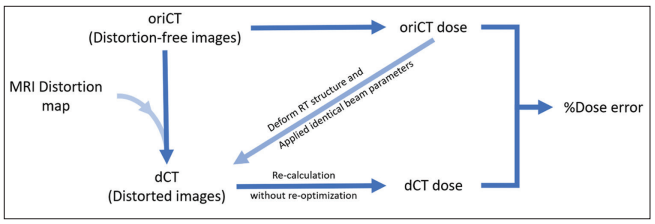

Figure 1: Schematic diagram of the distorted computed tomography generation and the percentage dose error (%Dose error) determination process. oriCT: Original computed tomography, dCT: Distorted computed tomography, MRI: Magnetic resonance imaging

The evaluation parameters are followed by ICRU-83.[18] These parameters included:

1. Near-minimum dose ($D_{98\%}$) of clinical target volume (CTV) and planning target volume (PTV)
2. Maximum dose (D_{max}) for CTV, PTV, rectum, bladder, and femoral head
3. Median dose ($D_{50\%}$) for PTV, rectum, and bladder
4. Absorbed dose in fraction 30% of volume (D30%) of the rectum and bladder.

The %Dose error values were computed for each of the mentioned evaluation parameters, comparing the doses obtained from the dCT with those from the oriCT using the DVH. Based on the dCT and oriCT images, this analysis provided insights into the accuracy of the radiation dose delivered to various anatomical structures.

Results

Geometric distortion

The residual distortions from GNL were plotted for all BWs at both phase-encoding directions, as presented in Figure 2. The distortion increases with an increasing distance from the bore isocenter. The mean distortion across the phantom was <2 mm at all conditions. The ranges of the mean, standard deviation, and maximum values for residual distortion are shown in Table 1. When comparing different BWs, higher BWs reduced distortion, predominantly affecting B_0 inhomogeneity rather than GNL, as described in Table 1. The result showed that the highest BWs reduced the distortion from 0.51 to 0.07 mm and 4.00 to 0.81 mm for the mean and maximum values, respectively.

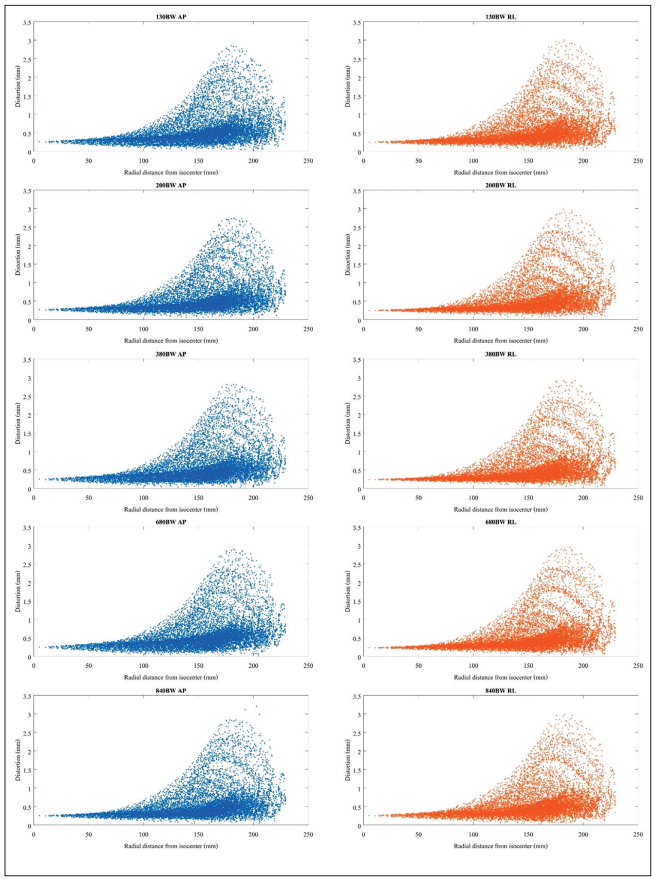

Figure 2: Scatter plot of the systemic geometric distortion as a result of the effect from gradient nonlinearity at varied bandwidths (Hz/pixel) for anteroposterior and right-to-left phase-encoding direction in a function of radial distance from magnet isocenter. AP: Anteroposterior, RL: Right to left

Impact on contour volume

The RT structures in the dCT plan were evaluated by calculating the DSC for each BW and phase-encoding direction to observe the impact of geometric distortion on the structures. The mean DSC was computed by averaging the DSC values across all 10 cases for each BW and phase-encoding direction. Structures failing to meet the criteria were excluded, and DSC averaging was performed for the remaining structures.

Across all BWs and both phase-encoding directions, the mean DSC values for the CTV and PTV ranged from 0.95–0.96 to 0.97–0.98, respectively. For all OARs except the rectum, the mean DSC exceeded 0.95. In comparison, the rectum's mean DSC ranged from 0.93 to 0.94. Notably, using higher BWs improved DSC values, indicating that higher BWs mitigated the distortion effects. Conversely, differences in phase-encoding directions did not exhibit impact. Additional details regarding DSC values for each structure are provided in Table 2.

Dosimetric accuracy

The %Dose error was assessed in accordance with ICRU-83. The analysis revealed that $D_{98\%}$ for CTV and PTV was below 2% for all BWs and phase-encoding directions. The highest observed error was 1.63% for $D_{98\%}$ at PTV, specifically for 130 Hz/pixel in the AP direction. In contrast, the CTV exhibited a minor variation between high and low BWs due to its central location. Simultaneously, distortion was more pronounced in

Table 1: The mean, standard deviation, and maximum of the systemic geometric distortions due to the gradient nonlinearity on the different bandwidths (Hz/pixel) and phase-encoding directions

BW (Hz/pixel)	Phase-encoding direction	GNL (mm)		B_0 inhomogeneity (mm)	
		Mean±SD	Maximum	Mean±SD	Maximum
130	AP	0.58±0.42	2.85	0.51±0.43	4.00
	RL	0.57±0.43	3.00	0.42±0.42	3.89
200	AP	0.58±0.41	2.74	0.41±0.28	2.68
	RL	0.56±0.43	2.98	0.27±0.27	2.50
380	AP	0.57±0.43	2.80	0.18±0.14	1.42
	RL	0.55±0.44	2.91	0.11±0.13	1.21
680	AP	0.58±0.43	2.89	0.08±0.07	0.72
	RL	0.55±0.44	2.94	0.08±0.07	0.65
840	AP	0.56±0.43	3.21	0.07±0.06	1.45
	RL	0.57±0.44	2.99	0.10±0.06	0.81

GNL: Gradient nonlinearity; BW: Bandwidth, AP: Anteroposterior, RL: Right to left, SD: Standard deviation

Table 2: Mean with±standard deviation of dice similarity coefficient for radiotherapy structures at different bandwidths and phase-encoding directions

Structure	Phase-encoding direction	DSC at Bws (Hz/pixel)				
		130	200	380	680	840
PTV	AP	0.97±0.01	0.97±0.01	0.97±0.01	0.97±0.01	0.97±0.01
CTV		0.95±0.01	0.95±0.02	0.95±0.01	0.95±0.01	0.95±0.02
Rectum*		0.93±0.02	0.93±0.02	0.93±0.02	0.93±0.02	0.94±0.03
Bladder		0.97±0.01	0.97±0.01	0.97±0.01	0.97±0.01	0.98±0.01
Femur left		0.96±0.01	0.96±0.01	0.96±0.01	0.96±0.01	0.97±0.01
Femur right		0.96±0.01	0.96±0.01	0.96±0.01	0.96±0.01	0.97±0.02
PTV	RL	0.97±0.01	0.97±0.01	0.97±0.00	0.98±0.01	0.98±0.01
CTV		0.95±0.01	0.95±0.01	0.95±0.01	0.96±0.02	0.95±0.02
Rectum*		0.93±0.02	0.93±0.02	0.93±0.02	0.94±0.03	0.94±0.03
Bladder		0.97±0.01	0.97±0.01	0.97±0.01	0.97±0.01	0.98±0.01
Femur left		0.96±0.01	0.97±0.01	0.96±0.01	0.97±0.01	0.97±0.01
Femur right		0.96±0.02	0.96±0.01	0.96±0.01	0.96±0.02	0.96±0.02

*One case was removed for the rectum because the DSC at bandwidths of 130, 200, 680, and 840 Hz/pixel at both phase-encoding directions was below the cutoff requirement. PTV: Planning target volume, CTV: Clinical target volume, AP: Anteroposterior, RL: Right to left, DSC: Dice similarity coefficient, BWs: BW: Bandwidths

the peripheral or distant regions from the isocenter. The $D_{50\%}$ and D_{max} at PTV showed that the %Dose error was <0.10% and 0.09% across all plans, respectively.

For the relevant OARs, the rectum exhibited %Dose errors beyond 2% for $D_{50\%}$ and $D_{30\%}$ in certain BWs. $D_{50\%}$ errors for 680 Hz/pixel in the RL direction reached up to 2.32%, and $D_{30\%}$ errors for 200 Hz/pixel in the AP direction reached up to 2.33%. However, the D_{max} for the rectum remained below 2% for all plans. In the case of the bladder, %Dose errors beyond 2% were observed for $D_{50\%}$, specifically 2.04%, 2.51%, 2.10%, and 2.08% for 130 (AP), 130 (RL), 380 (AP), and 680 (AP) Hz/pixel, respectively. Concerning both femurs, the %Dose error for D_{max} remained below 2% for all plans. Table 3 provides an overview of the dosimetric errors.

Discussion

Patients with prostate cancer would benefit from MRI-only treatment planning to reduce errors from CT/MRI registration. Furthermore, this approach eliminates the need for radiation dose and costs associated with CT simulation.[1] However, concerns persist regarding geometric distortion inherent to MRI. GNL was considered the main factor of the SGD. In addition, various parameters and phantom types also contributed to the magnitude of distortion.[7] In this study, the SGD from the GNL on 1.5T MRI simulation was quantified while excluding distortion from B_0 inhomogeneity. To achieve this, the QUASAR™ MRID^{3D} geometric distortion phantom was employed, utilizing the inverse gradient method to extract GNL without interference from other sources.[11] This approach overcomes the limitations observed in the study by Gustafsson *et al*., in which their results were influenced by a combination of OID and SGD from phantom.[3]

The results demonstrated that the mean residual distortion, both from GNL and B_0 inhomogeneity, met the American College of Radiology quality assurance (QA) criteria, which stipulates that distortion should be <2 mm.[19] Consistent with the AAPM-TG 284 recommendations, the inverse gradient method was employed to evaluate SGD. The study aligned with the first but not the second criterion due to the smaller size of the phantom.[16] The observed increase in SGD with greater distance from the isocenter aligns with expectations and corroborated previous findings.[3,4,8,20] Fatemi *et al*.[20] reported a mean distortion of 2.79 mm for a similar phantom and MRI model with a BW of 120 Hz/pixel, which contrasts with our results, showing a mean magnitude lower than 1 mm for a BW of 130 Hz/pixel. Differences in magnetic resonance parameters and machine-specific factors can contribute to variations in distortion magnitude, even among the same model.[20] The study revealed that higher BWs contributed to reduced distortion, particularly for B_0 inhomogeneity. However, this reduction was accompanied by a decrease in signal-to-noise ratio and an increase in scan time.[7,8,21] While such considerations are manageable in a phantom-based study, they may be more limited in clinical settings due to patient comfort and image quality requirements. In this study, the phase-encoding direction was varied between AP and RL directions, and the results showed that they were slightly different because the phantom dimension is a cylindrical shape with the same diameter along the axial plane (z-axis). On the other hand, when the phantom dimension has a longer side than the other, the effect increases the distortion on the longer side of the phantom.[22]

The impact of structure volume was evaluated with DSC between oriCT and dCT structures. The RT structure of the dCT plan simulated the effect of distortion by DIR on TPS. The DSC was similar in the different BWs with the same RT structure. The only effect on the bandwidths was due to B_0 inhomogeneity [as shown in Table 1], which was excluded from the distortion map. As a result, the RT structure of dCT was adopted from

Table 3: Mean with±standard deviation of percentage dose error for radiotherapy structure at different bandwidths and phase-encoding direction

BWs (Hz/pixel)	Dose parameter (%)	Percentage dose error (%Dose error)											
		AP phase-encoding direction						RL phase-encoding direction					
		PTV	CTV	Rectum*	Bladder	Femur left	Femur right	PTV	CTV	Rectum*	Bladder	Femur left	Femur right
130	$D_{98\%}$	1.63±1.72	0.06±0.08	-	-	-	-	1.14±0.68	0.07±0.07	-	-	-	-
	$D_{50\%}$	0.09±0.08	-	2.19±1.10	2.04±1.75	-	-	0.09±0.07	-	2.21±1.02	2.51±1.99	-	-
	$D_{30\%}$	-	-	1.94±1.15	1.77±1.85	-	-	-	-	1.80±1.36	1.00±1.58	-	-
	D_{max}	0.08±0.09	0.10±0.11	0.21±0.23	0.23±0.20	0.62±0.60	1.09±0.67	0.08±0.09	0.09±0.11	0.58±1.16	0.26±0.21	0.60±0.62	1.04±0.68
200	$D_{98\%}$	1.12±0.96	0.06±0.08	-	-	-	-	1.24±0.81	0.18±0.36	-	-	-	-
	$D_{50\%}$	0.09±0.07	-	1.85±1.43	1.77±1.54	-	-	0.08±0.08	-	2.27±1.47	1.58±1.66	-	-
	$D_{30\%}$	-	-	2.33±2.39	1.77±1.52	-	-	-	-	2.15±1.65	1.36±1.29	-	-
	D_{max}	0.08±0.10	0.10±0.12	0.22±0.27	0.25±0.23	0.60±0.65	0.73±0.60	0.07±0.09	0.07±0.09	0.16±0.15	0.24±0.19	0.59±0.67	1.01±0.72
380	$D_{98\%}$	0.97±1.00	0.08±0.09	-	-	-	-	1.63±1.80	0.07±0.08	-	-	-	-
	$D_{50\%}$	0.09±0.07	-	1.87±1.35	2.10±1.95	-	-	0.09±0.07	-	1.65±1.39	1.97±1.68	-	-
	$D_{30\%}$	-	-	1.39±0.92	1.79±1.79	-	-	-	-	2.14±2.84	1.86±2.09	-	-
	D_{max}	0.09±0.10	0.07±0.10	0.18±0.16	0.49±0.56	0.54±0.65	0.77±0.64	0.07±0.09	0.10±0.11	0.15±0.18	0.24±0.24	0.49±0.49	0.91±0.67
680	$D_{98\%}$	1.33±0.91	0.06±0.08	-	-	-	-	0.98±0.84	0.07±0.08	-	-	-	-
	$D_{50\%}$	0.09±0.08	-	1.84±1.20	2.08±1.83	-	-	0.09±0.07	-	2.32±2.42	1.72±1.55	-	-
	$D_{30\%}$	-	-	2.22±1.89	1.87±1.71	-	-	-	-	1.83±1.97	1.17±1.25	-	-
	D_{max}	0.09±0.10	0.10±0.11	0.24±0.21	0.22±0.19	0.54±0.67	1.03±0.64	0.08±0.09	0.10±0.11	0.21±0.25	0.20±0.20	0.54±0.65	0.89±0.71
840	$D_{98\%}$	0.94±0.79	0.08±0.07	-	-	-	-	0.98±0.92	0.09±0.08	-	-	-	-
	$D_{50\%}$	0.10±0.07	-	1.68±1.42	1.37±1.46	-	-	0.10±0.08	-	1.34±1.08	1.39±1.55	-	-
	$D_{30\%}$	-	-	1.56±1.59	0.86±1.22	-	-	-	-	1.26±1.43	0.97±1.22	-	-
	D_{max}	0.08±0.10	0.10±0.12	0.19±0.23	0.24±0.28	0.64±0.71	0.91±0.72	0.08±0.10	0.10±0.10	0.20±0.17	0.22±0.21	0.61±0.67	0.74±0.70

*One case was removed for the rectum because the DSC at bandwidths of 130, 200, 680, and 840 Hz/pixel at both phase-encoding directions was below the cutoff requirement. BWs: Bandwidths, $D_{98\%}$: Near-minimum dose, $D_{50\%}$: Median dose, $D_{30\%}$: Absorbed dose in fraction 30% of volume, D_{max}: Maximum dose, PTV: Planning target volume, CTV: Clinical target volume, AP: Anteroposterior, RL: Right to left, DSC: Dice similarity coefficient

the original plan. We found that in some cases, the DSC was lower than the criteria. Thus, the deformation algorithm was considered. The deformation algorithm used in this study was the demon algorithm (clinical routine in our hospital), which is based on the intensity difference between the two datasets, which would be a problem in homogeneous tissue, such as a pelvic area.[23,24] This point corresponds with Varadhan *et al*., which studied the accuracy of RT structure after DIR on prostate cancer patients and reported that the demon algorithm has a low DSC and performs worse at the rectum. For that reason, it was ambiguous to identify the impact on RT structure. Hence, another algorithm such as B-spline deformation should be used to limit the factor from the deformation algorithm error on a homogeneous area.[25]

To ensure that the beam parameter and couch structure of the dCT plan were identical to the oriCT plan for comparison, the dosimetric accuracy needed to be evaluated. Moreover, the center of images between the patient CT set and the distortion map must match the generated distorted plan, which would otherwise distort the air instead.[21] The %Dose error in this study was within 2% for CTV, PTV, and both femurs at all conditions, which is consistent with prior reports.[22,26] Exceptions were observed in some cases for the bladder and rectum, particularly for $D_{50\%}$ and $D_{30\%}$ where deviations above 2% were noted. These parameters are sensitive to changes in volume as the dose is averaged across the volume of interest. On the other hand, the D_{max} of all structures and conditions was 1% lower, reflecting its representation of a point dose and its insensitivity to volume changes.[27] In this study, the overall %Dose error was higher than that of the other reports,[3,22,28] while the DIR algorithm may not be suitable for the homogeneous area as mentioned above. In contrast, Adjeiwaah *et al*.,[22] Gustafsson *et al*.,[3] and Kemppainen *et al*.[28] utilized B-spline interpolation. To address this limitation, a pilot case was selected to compare the performance of the demon algorithm used in this study with the B-spline algorithm. The comparison demonstrated that using the B-spline algorithm improved the DSC of the rectum from 0.88–0.91 to 0.93–0.94, meeting the cutoff criteria. This improvement was consistent with the finding of Varadhan *et al*., indicating the potential benefits of further investigation, including gamma analysis, to evaluate radiation dose distribution. Furthermore, while this study solely evaluated the dosimetric impact of SGD induced by GNL, the potential effects of combined GNL and B_0 inhomogeneity were not explored. Such a combination is anticipated to increase in %Dose error.[22]

Conclusion

The utilization of MRI-only radiotherapy raises concerns regarding geometric distortion, as it has the potential to alter a patient's anatomy and lead to discrepancies in dose delivery. Therefore, SGD quantification is critical to understand its limitations, monitor machine performance, and assess its impact on dosimetric accuracy. Our results revealed that the mean residual SGD across all BWs and phase-encoding directions aligned with recommendations and findings from various studies. Overall, the %Dose error of all RT structures remained within 2%, with exceptions noted in the rectum and bladder in certain instances. However, these deviations were minor. In conclusion, the study supports the use of 1.5T MRI simulation for MRI-only treatment planning in prostate cancer patients. It highlights the importance of employing appropriate (QA) programs and parameter optimization to ensure clinically acceptable results, ultimately enhancing treatment efficiency and patient outcomes.

Acknowledgments

The authors express their sincere gratitude to all staff members at the Department of Radiology, Faculty of Medicine Ramathibodi Hospital, Mahidol University, for their invaluable guidance, support, and assistance throughout this research.

Financial support and sponsorship

Nil.

Conflicts of interest

There are no conflicts of interest.

References

1. Chandarana H, Wang H, Tijssen RHN, Das IJ. Emerging role of MRI in radiation therapy. J Magn Reson Imaging 2018;48:1468-78.
2. Owrangi AM, Greer PB, Glide-Hurst CK. MRI-only treatment planning: Benefits and challenges. Phys Med Biol 2018;63:05TR01.
3. Gustafsson C, Nordström F, Persson E, Brynolfsson J, Olsson LE. Assessment of dosimetric impact of system specific geometric distortion in an MRI only based radiotherapy workflow for prostate. Phys Med Biol 2017;62:2976-89.
4. Alzahrani M, Broadbent DA, Chuter R, Al-Qaisieh B, Jackson S, Michael H, *et al.* Audit feasibility for geometric distortion in magnetic resonance imaging for radiotherapy. Phys Imaging Radiat Oncol 2020;15:80-4.
5. Persson E, Jamtheim Gustafsson C, Ambolt P, Engelholm S, Ceberg S, Bäck S, *et al.* MR-PROTECT: Clinical feasibility of a prostate MRI-only radiotherapy treatment workflow and investigation of acceptance criteria. Radiat Oncol 2020;15:77.
6. Jonsson J, Nyholm T, Söderkvist K. The rationale for MR-only treatment planning for external radiotherapy. Clin Transl Radiat Oncol 2019;18:60-5.
7. Weygand J, Fuller CD, Ibbott GS, Mohamed AS, Ding Y, Yang J, *et al.* Spatial precision in magnetic resonance imaging-guided radiation therapy: The role of geometric distortion. Int J Radiat Oncol Biol Phys 2016;95:1304-16.
8. Walker A, Liney G, Metcalfe P, Holloway L. MRI distortion: Considerations for MRI based radiotherapy treatment planning. Australas Phys Eng Sci Med 2014;37:103-13.
9. Han S, Yin FF, Cai J. Evaluation of dosimetric uncertainty caused by MR geometric distortion in MRI-based liver SBRT treatment planning. J Appl Clin Med Phys 2019;20:43-50.
10. Pappas EP, Alshanqity M, Moutsatsos A, Lababidi H, Alsafi K, Georgiou K, *et al.* MRI-related geometric distortions in stereotactic radiotherapy treatment planning: Evaluation and dosimetric impact. Technol Cancer Res Treat 2017;16:1120-9.
11. Baldwin LN, Wachowicz K, Thomas SD, Rivest R, Fallone BG. Characterization, prediction, and correction of geometric distortion in 3 T MR images. Med Phys 2007;34:388-99.
12. Priola AM, Gned D, Veltri A, Priola SM. Chemical shift and diffusion-weighted magnetic resonance imaging of the anterior mediastinum in oncology: Current clinical applications in qualitative

and quantitative assessment. Crit Rev Oncol Hematol 2016;98:335-57.
13. Hood MN, Ho VB, Smirniotopoulos JG, Szumowski J. Chemical shift: The artifact and clinical tool revisited. Radiographics 1999;19:357-71.
14. Bley TA, Wieben O, François CJ, Brittain JH, Reeder SB. Fat and water magnetic resonance imaging. J Magn Reson Imaging 2010;31:4-18.
15. Eustace S, Goldberg R, Williamson D, Melhem ER, Oladipo O, Yucel EK, *et al.* MR imaging of soft tissues adjacent to orthopaedic hardware: Techniques to minimize susceptibility artefact. Clin Radiol 1997;52:589-94.
16. Glide-Hurst CK, Paulson ES, McGee K, Tyagi N, Hu Y, Balter J, *et al.* Task group 284 report: Magnetic resonance imaging simulation in radiotherapy: Considerations for clinical implementation, optimization, and quality assurance. Med Phys 2021;48:e636-70.
17. Brock KK, Mutic S, McNutt TR, Li H, Kessler ML. Use of image registration and fusion algorithms and techniques in radiotherapy: Report of the AAPM radiation therapy committee task group no. 132. Med Phys 2017;44:e43-76.
18. Hodapp N. The ICRU report 83: Prescribing, recording and reporting photon-beam intensity-modulated radiation therapy (IMRT). Strahlenther Onkol 2012;188:97-9.
19. American College of Radiology. Magnetic Resonance Imaging Quality Control Manual; 2015. Available from: https://www.acr.org/-/media/ACR/Files/Clinical-Resources/QC-Manuals/MR_QCManual.pdf. [Last accessed on 2022 Dec 29].
20. Fatemi A, Taghizadeh S, Yang CC, R Kanakamedala M, Morris B, Vijayakumar S. Machine-specific magnetic resonance imaging quality control procedures for stereotactic radiosurgery treatment planning. Cureus 2017;9:e1957.
21. Adjeiwaah M, Bylund M, Lundman JA, Söderström K, Zackrisson B, Jonsson JH, *et al.* Dosimetric impact of MRI distortions: A study on head and neck cancers. Int J Radiat Oncol Biol Phys 2019;103:994-1003.
22. Adjeiwaah M, Bylund M, Lundman JA, Karlsson CT, Jonsson JH, Nyholm T. Quantifying the effect of 3T magnetic resonance imaging residual system distortions and patient-induced susceptibility distortions on radiation therapy treatment planning for prostate cancer. Int J Radiat Oncol Biol Phys 2018;100:317-24.
23. Rigaud B, Simon A, Castelli J, Lafond C, Acosta O, Haigron P, *et al.* Deformable image registration for radiation therapy: Principle, methods, applications and evaluation. Acta Oncol 2019;58:1225-37.
24. Wang H, Dong L, O'Daniel J, Mohan R, Garden AS, Ang KK, *et al.* Validation of an accelerated 'demons' algorithm for deformable image registration in radiation therapy. Phys Med Biol 2005;50:2887-905.
25. Varadhan R, Karangelis G, Krishnan K, Hui S. A framework for deformable image registration validation in radiotherapy clinical applications. J Appl Clin Med Phys 2013;14:4066.
26. Bird D, Henry AM, Sebag-Montefiore D, Buckley DL, Al-Qaisieh B, Speight R. A Systematic review of the clinical implementation of pelvic magnetic resonance imaging-only planning for external beam radiation therapy. Int J Radiat Oncol Biol Phys 2019;105:479-92.
27. Yan Y, Yang J, Beddar S, Ibbott G, Wen Z, Court LE, *et al*. A methodology to investigate the impact of image distortions on the radiation dose when using magnetic resonance images for planning. Phys Med Biol 2018;63:085005.
28. Kemppainen R, Suilamo S, Ranta I, Pesola M, Halkola A, Eufemio A, *et al.* Assessment of dosimetric and positioning accuracy of a magnetic resonance imaging-only solution for external beam radiotherapy of pelvic anatomy. Phys Imaging Radiat Oncol 2019;11:1-8.